

Title	The STX6-VTI1B-VAMP3 complex facilitates xenophagy by regulating the fusion between recycling endosomes and autophagosomes
Author(s)	Nozawa, Takashi; Minowa-Nozawa, Atsuko; Aikawa, Chihiro; Nakagawa, Ichiro
Citation	Autophagy (2017), 13(1): 57-69
Issue Date	2017-01-02
URL	<a href="http://hdl.handle.net/2433/226849">http://hdl.handle.net/2433/226849</a>
Right	This is an Accepted Manuscript of an article published by Taylor & Francis in 'Autophagy' on 02 January 2017, available online: <a href="https://www.tandfonline.com/10.1080/15548627.2016.1241924">https://www.tandfonline.com/10.1080/15548627.2016.1241924</a> ; The full-text file will be made open to the public on 02 January 2018 in accordance with publisher's 'Terms and Conditions for Self-Archiving'.; This is not the published version. Please cite only the published version. この論文は出版社版ではありません。引用の際には出版社版をご確認ご利用ください。
Type	Journal Article
Textversion	author

The STX6-VTI1B-VAMP3 complex facilitates xenophagy by regulating the fusion between recycling endosomes and autophagosomes

### **Authors and affiliations**

Takashi Nozawa, Atsuko Minowa-Nozawa, Chihiro Aikawa, and Ichiro Nakagawa \*

Department of Microbiology, Graduate School of Medicine, Kyoto University,

Yoshida-Konoe-cho, Sakyo-ku, Kyoto 606-8501, Japan

### **Contact**

\*Correspondence: Ichiro Nakagawa

E-mail: nakagawa.ichiro.7w@kyoto-u.ac.jp

**Abbreviations:** GAS, Group A *Streptococcus*; GcAV, GAS-containing autophagosome-like vacuole; RE, recycling endosome; SNARE, soluble *N*-ethylmaleimide-sensitive factor attachment protein receptor; EmGFP, emerald green fluorescent protein; TGN, *trans*-Golgi network;. MAP1LC3B/LC3B, microtubule-associated protein 1 light chain 3  $\beta$  (a mammalian ortholog of yeast Atg8); TM, transmembrane; BSA, bovine serum albumin; DAPI, 4',6-diamidino-2-phenylindole.

## Abstract

Autophagy plays a critical role in immunity by directly degrading invading pathogens such as Group A *Streptococcus* (GAS), a process that has been named xenophagy. We previously demonstrated that autophagic vacuoles directed against GAS, termed GAS-containing autophagosome-like vacuoles (GcAVs), use recycling endosomes (REs) as a membrane source. However, the precise molecular mechanism that facilitates the fusion between GcAVs and REs remains unclear. Here, we demonstrate that STX6 (syntaxin 6) is recruited to GcAVs and forms a complex with VTI1B and VAMP3 to regulate the GcAV-RE fusion that is required for xenophagy. STX6 targets the GcAV membrane through its tyrosine-based sorting motif and transmembrane domain, and localizes to TFRC (transferrin receptor)-positive punctate structures on GcAVs through its H2 SNARE domain. Knockdown and knockout experiments revealed that STX6 is required for the fusion between GcAVs and REs to promote clearance of intracellular GAS by autophagy. Moreover, VAMP3 and VTI1B interact with STX6 and localize on the TFRC-positive puncta on GcAVs, and are also involved in the RE-GcAV fusion. Furthermore, knockout of RABGEF1 impairs the RE-GcAV fusion and STX6-VAMP3 interaction. These findings demonstrate that RABGEF1 mediates RE fusion with GcAVs through the STX6-VAMP3-VTI1B complex, and reveal the SNARE dynamics involved in autophagosome formation in response to bacterial infection.

- 1 **Keywords:** Autophagy, Group A *Streptococcus*, STX6 (syntaxin 6), RABGEF1/RABEX5,
- 2 Xenophagy

## 1    **Introduction**

2    Autophagy is a lysosomal degradation pathway that degrades cytoplasmic components,  
3    including protein aggregates, damaged organelles, and invading bacteria. This pathway is  
4    essential for cellular homeostasis, survival, development, and host defense. During autophagy,  
5    a flat membrane structure, called the isolation membrane, is generated from or close to the  
6    endoplasmic reticulum and surrounds a portion of the cytoplasmic content and forms a closed  
7    double-membrane structure, the autophagosome. The process of autophagosome formation is  
8    regulated by autophagy-related (Atg) proteins, and one of the Atg proteins, LC3 (mammalian  
9    homolog of Atg8 in yeast), specifically localizes on autophagosomes; the autophagosomes  
10    subsequently fuse with lysosomes and form the autolysosome, a lysosomal vacuole in which  
11    the autophagosome contents are degraded.<sup>1, 2</sup>

12            Autophagy not only degrades a cell's own components, but also targets invading  
13    microbial pathogens. This antimicrobial autophagy, which is named xenophagy,<sup>3, 4</sup> has been  
14    recognized as a crucial intracellular immune system against various pathogens, such as  
15    *Salmonella* Typhimurium and Group A *Streptococcus* (GAS).<sup>4, 5</sup> GAS, one of the major  
16    human pathogens, enters epithelial cells through endocytosis and then escapes into the  
17    cytoplasm by secreting streptolysin O, a pore-forming toxin produced by GAS.<sup>6</sup> The exposed  
18    GAS in the cytoplasm is recognized by the ubiquitin and adaptor proteins SQSTM1/p62 and

CALCOCO2/NDP52 pathway and entrapped by an LC3-positive autophagic membrane structure, the GAS-containing autophagosome-like vacuole (GcAV). RAB7 and RAB9A facilitate the homotypic fusion between GcAVs that generates large GcAVs,<sup>7, 8</sup> and RAB9A mediates the fusion of GcAVs with lysosomes, which results in the degradation of the entrapped bacteria.<sup>8</sup> Recently, we showed that forming (unclosed) GcAV membranes contain punctate structures that are derived from recycling endosomes (REs).<sup>9</sup> Moreover, we found that RAB17-mediated RE recruitment into GcAVs promoted the formation of GcAVs and the elimination of intracellular bacteria, which suggested that the RE functions as a primary membrane source for—and is critical for—autophagosome formation during xenophagy.<sup>9</sup> However, the mechanism of RE fusion with GcAVs remains unclear, and elucidation of this mechanism is crucial for understanding xenophagy.

Specific membrane-fusion events in diverse vesicle-mediated transport pathways are typically regulated by soluble *N*-ethylmaleimide-sensitive factor attachment protein receptor (SNARE) complexes.<sup>10</sup> At the membrane-fusion step, the SNARE complex forms parallel 4-helix bundles comprising the Qa-, Qb-, Qc-, and R-SNAREs. To date, several SNAREs have been shown to function in autophagy in mammals: STX17 (syntaxin 17), SNAP-29, VAMP8, VTI1B, and VAMP7 are required for lysosome-autophagosome fusion,<sup>11</sup> and VAMP8 and VTI1B are also used in GcAV-lysosome fusion.<sup>12</sup> Furthermore, in yeast, Vam3, Vam7, Ykt6, and Vti1 have been identified to regulate lysosomal fusion.<sup>13, 14</sup> With

1 regard to the autophagosome formation process preceding lysosomal fusion, previous studies  
2 have reported that VAMP3 mediates heterotypic fusion between ATG9- and  
3 ATG16L1-positive vesicles for autophagosome precursor formation,<sup>15</sup> and that yeast Sec22,  
4 Ykt6, Tlg2, Sec9, and Sso1 are required for isolation membrane biogenesis.<sup>16</sup> Thus,  
5 identifying the SNARE complex that functions in the RE-autophagosome fusion step is  
6 critical for understanding not only xenophagy, but also the fundamental autophagosome  
7 formation mechanism in mammals.

8           In this study, to identify the SNARE complex that is involved in  
9 RE-autophagosome fusion during bacterial infection, we examined the subcellular  
10 localization of STX-family proteins during GAS infection. We report that STX6 localizes to  
11 RE-derived punctate structures on GcAVs and is recruited to GcAVs in response to GAS  
12 infection, and that STX6 knockout impairs RE recruitment to GcAVs and suppresses GcAV  
13 formation. Furthermore, we show that VAMP3 and VTI1B function together with STX6 in  
14 RE-GcAV fusion.

## Results

### *STX6 localizes to TFRC-positive puncta on GcAVs during GAS infection*

To identify the SNARE proteins that mediate RE-GcAV fusion, we examined the localization of EmGFP-fused STX proteins and the autophagosomal marker MAP1LC3B/LC3B during GAS infection in HeLa cells. Out of 11 STX proteins, 5 (STX6, STX10, STX11, STX12, and STX17) were found to clearly colocalize with GAS-surrounding LC3-positive vacuoles (GcAVs) (Fig. S1). We counted the EmGFP-STX-positive GcAVs and determined that EmGFP-STX6 most frequently colocalized with GcAVs ( $61.5\% \pm 5.8\%$ ) (Fig. 1A). To confirm the GcAV localization of STX6, we examined the subcellular localization of endogenous STX6 during GAS infection. STX6 was detected around GAS and colocalized with GcAVs (Fig. 1B). Furthermore, EmGFP-STX6 showed punctate localization on forming (unclosed) GcAVs (Fig. 1C), and the GcAV colocalization frequency increased with time after infection (Fig. 1D). Next, we examined STX6 colocalization with TFRC, an RE marker, in GAS-infected cells, and found that EmGFP-STX6 clearly colocalized with TFRC on GcAVs (Fig. 1E). To determine whether STX6 preferentially colocalizes with TFRC on GcAVs, we calculated the Pearson's coefficient for colocalization from the GcAV images: STX6 showed significantly higher colocalization with TFRC than with LC3 on GcAVs (Fig. 1F). Furthermore, the signal-intensity plot (Fig. 1G) of STX6 and TFRC together with GcAVs (red line in the figure) revealed coincident signal peaks (orange arrows). These results demonstrate



1 that STX6 colocalizes with TFRC-positive punctate structures on GcAVs. We also performed  
2 time-lapse imaging of cells during GAS infection and examined EmGFP-STX6 recruitment  
3 into GcAVs. We found that bacteria-containing LC3-positive vacuoles acquired punctate  
4 EmGFP-STX6 with time (Fig. 1H), indicating that STX6 is recruited to autophagosomes  
5 during GAS infection.

### 7 ***STX6 is involved in RE-GcAV fusion***

8 Because STX6 localized to TFRC-positive puncta on GcAVs, we next knocked down STX6  
9 expression (Fig. 2A) and determined whether STX6 is required for RE-GcAV fusion and  
10 GcAV formation: STX6 knockdown led to a reduction in TFRC-positive GcAVs (Fig. 2B and  
11 2C). We also constructed an STX6-knockout HeLa cell line by using the CRISPR/Cas9  
12 genome-editing system (Fig. 2D),<sup>17</sup> and found that in these STX6-knockout cells, the TFRC  
13 signal was rarely detected on GcAVs (Fig. 2E and 2F). Furthermore, in rescue experiments,  
14 FLAG-STX6 expression in the STX6-knockout HeLa cells increased RE recruitment to  
15 GcAVs (Fig. 2F). To investigate the effects of STX6 knockout on transferrin uptake and the  
16 endocytosis pathway associated with TFRC, we treated cells with Alexa-594-labelled human  
17 transferrin and observed internalized transferrin, and also examined the subcellular  
18 localization of TFRC in STX6-knockout cells. In our experiments, transferrin was normally  
19 internalized (Fig. S2A), and TFRC frequently colocalized with RAB17 in the perinuclear

1 region and partially overlapped with TGOLN2/TGN46 (TGN marker) in STX6-knockout  
2 cells (Fig. S2B and S2C). These knockdown and knockout results clearly demonstrate that  
3 STX6 functions in RE-GcAV fusion.

4 RE recruitment to GcAVs involves RAB17 and RABGEF1, and RAB17  
5 inactivation reduces GcAV formation; these findings indicate that REs promote GcAV  
6 formation. Thus, to determine whether STX6-mediated RE fusion is involved in GcAV  
7 formation, we quantified GcAV formation efficiency in wild-type and STX6-knockout HeLa  
8 cells: The characteristic large GcAVs were detected only in wild-type cells (Fig. 2G), and  
9 significantly fewer STX6-knockout cells were GcAV-positive as compared to wild-type cells  
10 (Fig. 2H). To ascertain whether or not the defective autophagosome formation in  
11 STX6-knockout cells affects the viability of intracellular GAS, we determined the number of  
12 surviving GAS. Although the number of invaded GAS was not altered, the number of  
13 recovered GAS at 4 h after infection significantly increased in STX6-knockout cells  
14 compared with wild-type cells (Fig. 2I). Collectively, our results suggest that RE-GcAV  
15 fusion involves STX6 and that this STX6-mediated fusion facilitates GcAV formation to  
16 restrict GAS proliferation in cells.

#### 18 ***VAMP3 and VTI1B function together with STX6***

19 Next, we searched for other SNARE proteins that function in the RE-GcAV fusion step

1 together with STX6. Previously, STX6 was found to associate with various SNARE proteins,  
2 such as VAMP7, VAMP8, VTI1A, and VTI1B, and was suggested to interact with distinct  
3 SNARE partners depending on the cell type examined.<sup>18</sup> Therefore, we screened for the  
4 SNARE proteins that localized to TFRC-positive puncta on GcAVs in HeLa cells; our results  
5 showed that 6 SNARE proteins colocalized with GcAVs (Fig. S3), and 2 of these proteins,  
6 VAMP3 and VTI1B, preferentially colocalized with TFRC on GcAVs, but not with LC3 on  
7 GcAVs (Fig. 3A–3C). Furthermore, immunoprecipitation analyses revealed that STX6  
8 interacts with VAMP3 and VTI1B during GAS infection (Fig. 3D).

9           To ascertain whether VAMP3 and VTI1B facilitate the fusion between REs and  
10 GcAVs, we knocked down the expression of these SNARE proteins (Fig. 3E). VAMP3  
11 knockdown inhibited the Golgi-like perinuclear compartment localization of transferrin (Fig.  
12 S4A). In contrast, VAMP3 and VTI1B knockdown did not affect transferrin uptake or  
13 colocalization between TFRC and RAB17 (Fig. S4A and S4B), suggesting that it did not  
14 profoundly affect RAB17-associated TFRC trafficking. However, knockdown of either  
15 VAMP3 or VTI1B significantly reduced the colocalization of TFRC and GcAVs (Fig. 3F and  
16 3G). Collectively, these results suggest that VAMP3 and VTI1B cooperate with STX6 in the  
17 RE-GcAV fusion process.

18  
19 ***H2 SNARE domain of STX6 is required for punctate localization on GcAVs and interaction***

1 ***with VAMP3 and VTI1B***

2 We next sought to identify the domains of STX6 that are responsible for its localization to  
3 GcAVs and the TFRC-positive punctate structures on GcAVs. The STX6 gene encodes a  
4 protein containing 255 amino acids, and the C-terminal 20 amino acids of STX6 are  
5 hydrophobic and form a transmembrane (TM) domain.<sup>18</sup> STX6 further contains 2 coiled-coil  
6 domains—H1 and H2—that have been implicated in mediating protein interactions,<sup>18</sup> and one  
7 tyrosine-based sorting motif (YGRL, residues 140–143). We constructed STX6 deletion  
8 mutants lacking the aforementioned domains (Fig. 4A) and quantified their GcAV  
9 colocalization in HeLa cells. Deletion of the TM domain suppressed STX6 targeting to all  
10 membranes, including GcAVs (Fig. 4B and 4C), which suggests that the TM domain is  
11 necessary for GcAV localization of STX6. Moreover, although STX6 166–255 and  $\Delta$ YGRL  
12 mutants appeared to retain their intracellular membrane localization, they also failed to  
13 localize to GcAVs (Fig. 4B and 4C). These results suggest that the YGRL sorting motif is  
14 required for GcAV targeting. Intriguingly, EmGFP-STX6  $\Delta$ H2 was detected on GcAVs but  
15 did not display the punctate localization, and this mutant showed higher colocalization with  
16 LC3 than did wild-type STX6 (Fig. 4B and 4C). Additionally, the signal peaks of  
17 EmGFP-STX6 $\Delta$ H2 did not coincide with those of TFRC on GcAVs (Fig. 4D). These results  
18 suggest that the H2 domain is required for the TFRC-positive punctate localization of STX6  
19 on GcAVs.

The H2 domain is also known as the SNARE core domain, and thus we performed immunoprecipitation assays by using the STX6 deletion mutants to examine the domain's role in STX6 interactions: VAMP3 precipitated with STX6 wild-type and  $\Delta$ H1 but not  $\Delta$ H2 (Fig. 4E), which suggested that the STX6 H2 domain interacts with VAMP3. Similarly, STX6  $\Delta$ H2 did not interact with VTI1B (Fig. 4E). To determine whether the H2 domain and YGRL motif are required for GcAV formation, we performed rescue experiments using these deletion constructs. Expression of full-length STX6 recovered GcAV formation efficiency in STX6-knockout cells, and this recovery was not observed in  $\Delta$ H2 or  $\Delta$ YGRL mutants (Fig. 4F). Taken together, our findings suggest that STX6 is recruited to GcAVs by the YGRL sorting motif and is localized in the membrane through its TM domain, and further that STX6 exhibits a punctate localization and interacts with other SNARE proteins through the H2 SNARE domain.

#### ***RABGEF1 is required for STX6-mediated RE-GcAV fusion***

We previously reported that RAB17 and RABGEF1 regulate RE recruitment into GcAVs and GcAV formation and thereby facilitate xenophagy.<sup>9</sup> In the present study, we investigated whether the STX6/VAMP3/VTI1B complex colocalizes with RAB17-positive vesicles. EmGFP-STX6 and -VAMP3 colocalized with mCherry-RAB17 in the perinuclear region and in many vesicles; however, VTI1B only colocalized with RAB17 in the perinuclear region

(Fig. S5). Thus, to determine whether RAB17/RABGEF1 and the STX6/VAMP3/VTI1B complex function in same pathway during GcAV formation, we generated a RABGEF1-knockout HeLa cell line (Fig. 5A) and analyzed the involvement of the STX6-VAMP3-VTI1B complex. First, we examined the colocalization of LC3 and TFRC during GAS infection, and found that the colocalization between GcAVs and TFRC was decreased in RABGEF1-knockout cells (Fig. 5B and 5C); furthermore, GcAV formation efficiency was also reduced in the knockout cells (Fig. 5D). Expression of RABGEF1 increased the numbers of both TFRC-positive GcAV and GcAV-positive cells among RABGEF1-knockout cells (Fig. 5B-5D), confirming that RABGEF1 facilitates RE-GcAV fusion and GcAV formation. These results agreed with the findings of our previous study.<sup>9</sup> Next, we analyzed the effects of RABGEF1 knockout on the GcAV localization of STX6, VAMP3, and VTI1B. Whereas EmGFP-STX6 and -VTI1B were detected on GcAVs at similar levels in wild-type and RABGEF1-knockout cells, EmGFP-VAMP3-positive GcAVs were rarely observed in the knockout cells (Fig. 5E). Quantification of the colocalization between EmGFP-SNAREs and GcAVs revealed that the colocalization of VAMP3 with GcAVs was substantially lower in RABGEF1-knockout cells than in control cells (Fig. 5F). These data suggest that VAMP3 recruitment to GcAVs is regulated by RABGEF1.

Furthermore, to ascertain whether STX6-VAMP3-VTI1B interactions are also regulated by RABGEF1, we performed immunoprecipitations with the RABGEF1-knockout

1 cells. Although the interaction between STX6 and VTI1B was almost equal in control and  
2 knockout cells, the association between STX6 and VAMP3 was substantially decreased in  
3 RABGEF1-knockout cells (Fig. 5G and 5H), which indicates that RABGEF1 is required for  
4 the interaction between STX6 and VAMP3. Collectively, these results suggest that VAMP3 is  
5 recruited to GcAVs through a RABGEF1-mediated pathway and forms a complex with STX6  
6 and thus mediates RE-GcAV fusion.

#### 7 8 ***STX6 but not RABGEF1 is involved in starvation-induced autophagosome formation***

9 Lastly, we examined the involvement of STX6 and RABGEF1 in autophagy during starvation.  
10 LC3-II levels increased under starvation or treatment with protease inhibitors (E64d and  
11 pepstatin A) in wild-type cells; however, STX6 knockout suppressed LC3-II accumulation  
12 under starvation and protease inhibitors treated conditions (Fig. 6A and 6B). This suggests  
13 that autophagosome formation was impaired. In contrast, the LC3-II level increased in  
14 response to starvation in RABGEF1-knockout cells (Fig. 6C and 6D), suggesting that  
15 RABGEF1 is dispensable for starvation-induced autophagosome formation.

16 In wild-type cells, the number of GFP-LC3 puncta increased during starvation (Fig.  
17 6E and 6F). The number of GFP-LC3 puncta also increased slightly even in STX6-knockout  
18 cells; however, the number was still significantly lower than that in wild-type cells (Fig. 6E  
19 and 6F). Taken together, these findings suggest that STX6 but not RABGEF1 is involved in

autophagosome formation under starvation conditions.

### Discussion

In this study, we showed that STX6 regulates the fusion between autophagosomes and REs and thereby promotes autophagosome biogenesis during xenophagy. STX6 targets the GAS-capturing, forming (unclosed) GcAVs through its tyrosine-based sorting motif and localizes to RE-derived punctate structures on GcAVs. VTI1B and VAMP3 also localize to this punctate structure, and the recruitment of VAMP3 depends on a RABGEF1-mediated RE-GcAV fusion pathway. Notably, the results of knockdown and knockout analysis showed that the STX6-VAMP3-VTI1B complex is required for the GcAV-RE fusion and GcAV formation necessary for xenophagy.

STX6 is widely recognized to participate in various fusion events.<sup>18</sup> However, this is the first report of STX6 involvement in autophagy. STX6 mainly localizes to the *trans*-Golgi network (TGN) and endosomal structures, and is suggested to regulate Glut4 trafficking,<sup>19</sup> the secretory pathway,<sup>20</sup> caveolar endocytosis,<sup>21</sup> and endosome-TGN retrograde transport.<sup>22</sup> TFRC-positive REs are also incorporated into starvation-induced autophagosomes and facilitate autophagosome formation, and their trafficking is regulated by TBC1D14 and RAB11.<sup>23</sup> However, the fusion of REs with GcAVs is mediated by RAB17 rather than RAB11,<sup>9</sup> and thus the SNARE machinery involved in the RE-autophagosome fusion step



1 might also differ between canonical autophagy and xenophagy.

2           We revealed the GcAV localization of STX6 in this study and identified the STX6  
3 domains required for the protein's targeting to and punctate localization on GcAVs. Because  
4 the number of STX6-positive GcAVs increased with time, STX6 is likely acquired by GcAVs  
5 and not initially contained in GcAV precursors. Notably, deletion of the tyrosine-based motif  
6 YRGL in STX6 prevented the recruitment of STX6 to GcAVs (Fig. 4B and 4C). The YGRL  
7 motif of STX6 functions in the return to the *trans*-Golgi from the plasma membrane,<sup>24</sup> and it  
8 is also required for targeting to the chlamydia inclusion membrane.<sup>25, 26</sup> Kabeiseman et al.  
9 suggested that deletion or alteration of the YGRL region does not markedly affect the protein  
10 interactions of STX6, but reduces the interaction with lipids such as phosphatidylinositol  
11 3-phosphate, phosphatidylinositol 4-phosphate, and phosphatidylinositol 5-phosphate.<sup>26</sup>  
12 Therefore, although it is not yet clear whether STX6 is recruited to GcAVs through lipid  
13 interactions, further investigation of the lipid contents of GcAVs should help enhance our  
14 understanding of STX6 recruitment.

15           We found that STX6 forms a complex with VTI1B and VAMP3 and that this  
16 complex defends cells through autophagy. Interestingly, STX6 and VTI1B have been reported  
17 to function as a part of the Q-SNARE complex (STX6-VAMP7-VTI1B) on the TGN together  
18 with the R-SNARE VAMP3 and thereby regulate TNF $\alpha$  trafficking in macrophages.<sup>27</sup>  
19 Moreover, the STX6-VTI1B-VAMP3 complex has been reported to regulate the IL-6

1 secretion pathway through REs in macrophages.<sup>28</sup> Because STX6 is suggested to change its  
2 SNARE partners and thus specifically regulate several different fusion events, the  
3 STX6-VTI1B-VAMP3 complex could be activated in response to pathogenic infection.  
4 Intriguingly, STX6 is a cholesterol-binding protein,<sup>29</sup> and alteration of the cholesterol level at  
5 the TGN/endosome boundary causes STX6 accumulation on VAMP3-positive REs.<sup>30</sup>  
6 Bacterial pathogens carry secreted toxins that interact with cholesterol and affect its  
7 intracellular balance,<sup>31, 32</sup> and streptolysin O, a cytolysin secreted by GAS, also interacts  
8 with cholesterol molecules in target bilayers and could affect cholesterol dynamics.<sup>33</sup> This  
9 raises the possibility that the STX6-VAMP3-VTI1B complex is activated in response to  
10 changes in cholesterol levels during bacterial infection.

11 VTI1B has been reported to be involved in the fusion between GcAVs and  
12 lysosomes, which suggests that VTI1B regulates multiple steps of the GcAV formation  
13 process. Furuta et al.<sup>12</sup> reported that VTI1B is recruited to GcAVs before lysosomal fusion,  
14 and our results also showed that VTI1B colocalized with forming (unclosed) GcAVs (Fig. 3C).  
15 However, VTI1B mainly localizes in the TGN and endosomes<sup>34</sup> and is recruited to GcAVs  
16 even in RABGEF1-knockout cells; thus, we suggest that VTI1B targets GcAVs through a  
17 pathway distinct from that used by VAMP3.

18 Although this finding is slightly out of the scope of the present study, we found that  
19 STX6 is required for autophagosome formation under starvation conditions (Fig. 6A, 6B, 6E

1 and 6F). Importantly, RABGEF1 was dispensable for starvation-induced autophagosome  
2 formation (Fig. 6C and 6D), in agreement with our previous data. Because STX6-mediated  
3 RE fusion involves RABGEF1, STX6 might be involved in canonical autophagy through a  
4 mechanism different from that involved in xenophagy. Zhang et al. reported that *O*-linked  
5  $\beta$ -*N*-acetylglucosamine transferase modifies the SNARE protein SNAP-29 in a  
6 nutrient-dependent manner and implied that the STX6-SNAP-29 complex is involved in  
7 autophagy induction.<sup>35, 36</sup> Considering our results regarding starvation-induced autophagy,  
8 STX6 may be an essential regulator in canonical autophagy.

9 In this study, we showed that GcAV localization was exhibited by 11 SNAREs  
10 (EmGFP-fused STX6, STX10, STX11, STX12, STX17, VAMP2, VAMP3, VAMP4, VAMP7,  
11 VAMP8, and VTI1B), but roles in GcAV formation have been identified for only 5 of these  
12 SNAREs; we have described the function of STX6. Our finding that several SNAREs localize  
13 on GcAVs suggests the involvement of multiple organelle-derived vesicles in GcAV  
14 formation, but the functions of other SNAREs in xenophagy remain unclear. Additional  
15 studies on SNAREs will not only help reveal the molecular mechanism of GcAV formation,  
16 but also enhance our understanding of canonical autophagy.

## 1    **Materials and Methods**

### 2    ***Cell culture and transfection***

3    HeLa cells were maintained in Dulbecco's modified Eagle's medium (DMEM; Nacalai  
4    Tesque, 18459-64) supplemented with 10% fetal bovine serum (FBS; Gibco) and 50 µg/mL  
5    gentamicin (Nacalai Tesque, 11980-14) in a 5% CO<sub>2</sub> incubator at 37°C. The transfection  
6    reagents used were polyethylenimine (Polysciences, 23966-2) and Lipofectamine 3000  
7    (Invitrogen Corporation, L3000001).

### 8    ***Bacterial strain***

9    GAS strain JRS4 (M6<sup>+</sup> F1<sup>+</sup>) was grown in Todd-Hewitt broth (BD Diagnostic Systems)  
10    supplemented with 0.2% yeast extract (THY) as described previously.<sup>6</sup>

### 11    ***Antibodies and other reagents***

12    The following primary antibodies were used: rabbit monoclonal anti-Syntaxin 6 (C34B2;  
13    2869), rabbit polyclonal anti-VAMP3 (13640), rabbit monoclonal anti-β-actin (D6A8; 8457),  
14    and rabbit monoclonal anti-RABGEF1 for Rabex5 (D21F12; 7622), from Cell Signaling  
15    Technology; rabbit polyclonal anti-VTI1B (Proteintech Group, 14495-1-AP); mouse  
16    monoclonal anti-CD71 (OX26) for TFRC (Santa Cruz Biotechnology, sc-53059); mouse  
17    monoclonal anti-FLAG (M2) (Sigma-Aldrich, A2220); and mouse monoclonal anti-GFP  
18    (GF200), (Nacalai Tesque, 04363-24). The secondary antibodies used were the following: for  
19    immunoblotting, HRP-conjugated anti-rabbit and anti-mouse IgG (Jackson ImmunoResearch

Laboratories, 111-035-144 and 115-035-003 respectively); for immunostaining, Cy5-goat anti-rabbit IgG (Jackson ImmunoResearch Laboratories, 711-175-152), and anti-mouse or anti-rabbit IgG conjugated with AlexaFluor-488/-594 (Invitrogen Corporation, A-11001, A-11008, A-11032, and A-21442). E64d (Enzo Life Sciences, BML-PI107-0001) and pepstatin A (Nacalai Tesque, 26305-03-3) were used at 10 µg/mL and 30 µg/mL, respectively.

### ***Plasmids***

Human SNARE cDNAs were PCR-amplified from HeLa, KYSE, and HEK293T cell total mRNAs and cloned into pcDNA-6.2/N-EmGFP-DEST (N-terminal tagged), pcDNA-6.2/N-3xFLAG-DEST (N-terminal tagged), and pcDNA-6.2/N-mCherry-DEST (N-terminal tagged) by using Gateway cloning technology as described previously.<sup>8</sup> A BLOCK-iT Pol II miR-RNAi expression vector kit (Invitrogen Corporation, K493500) was used to knockdown STX6, VAMP3, and VTI1B expression. We used the following targeting sequences: STX6, 5'-TACAAGTACTCGGCAAGTTGT-3'; VAMP3, 5'-TGGCAGTAATCGAAGACTTCA-3'; and VTI1B, 5'-GATGTCTAAGCTTCGAAACTA-3'. The miRNA double-strand sequences were ligated to pcDNA-6.2-GW/miR, as per supplier instructions; pcDNA6.2-GW/miR-neg was used as the miRNA control. These plasmids were transfected into HeLa cells as described above. Knockdowns were confirmed through immunoblotting.

1     ***Generation of knockout lines by using CRISPR/Cas9 gene editing***

2     We used the CRISPR/Cas9 system to generate STX6- and RABGEF1-knockout cell lines, as  
3     described previously.<sup>37</sup> Briefly, CRISPR guide RNAs (gRNAs) were selected that targeted an  
4     exon common to all splicing variants of the gene of interest (STX6:  
5     ATGTCAACTTCATCTGTGC; RABGEF1: TCTCATCATCAGTAGTTTC). For  
6     CRISPR/Cas9 gene editing, HeLa cells were transfected with the gRNA-hyg vector  
7     containing CRISPR target sequences and hCAS9<sup>17</sup> (Addgene, 41815, George Church Lab).  
8     After the transfection step, untransfected cells were removed through selection with 300  
9     µg/mL hygromycin B and 750 µg/mL geneticin (G418) (both from Nacalai Tesque, 09287-84  
10    and 16513-26 respectively). Single colonies were expanded and the depletion of the targeted  
11    gene product was confirmed through immunoblotting. As a secondary screen of certain  
12    knockout lines, genomic DNA was isolated from cells and the genomic regions of interest  
13    were amplified using PCR. The targeted genomic regions of the knockout lines were also  
14    sequenced to confirm the presence of frameshifting indels in the genes of interest.

15    ***Generation of cell lines with stable transgene expression***

16    Cell lines with stable transgene expression were generated by retroviral infection as  
17    previously described. Based on pLenti6/V5-DEST, the virus was produced using the  
18    ViraPower lentiviral expression system (Invitrogen Corporation, K4960-00) according to the  
19    manufacturer's protocol. Briefly, 293 FT cells were cotransfected with pLenti-EmGFP-LC3

1 and the mixture of packaging plasmids (Invitrogen Corporation, K4975-00) using  
2 Lipofectamine 3000, and then cultured for 48 h. The viral supernatant was collected and used  
3 to infect HeLa cells. After 24 h, uninfected cells were removed by selection on 5 µg/mL  
4 blasticidin (Invitrogen Corporation, A1113903).

### 5 ***Bacterial infection***

6 Cells were infected with GAS as described previously.<sup>6</sup> Briefly, bacteria were incubated with  
7 cell cultures for 1 h at a multiplicity of infection of 100 in the absence of antibiotics. The  
8 infected cells were washed with phosphate-buffered saline (PBS; 137 mM NaCl, 2.7 mM KCl,  
9 8.1 mM Na<sub>2</sub>HPO<sub>4</sub>, 1.47 mM KH<sub>2</sub>PO<sub>4</sub> [pH 7.4]) and the antibiotic gentamicin (100 µg/mL)  
10 was added for an appropriate period to kill extracellular bacteria.

### 11 ***Fluorescence microscopy and image analyses***

12 For confocal microscopy analysis, cells were cultured on 12-mm-diameter glass coverslips in  
13 24-well culture plates. The cells were placed on a glass-bottom dish to facilitate time-lapse  
14 imaging. For immunostaining, cells were washed with PBS, fixed with 4% paraformaldehyde  
15 in PBS for 15 min, permeabilized with 0.1% Triton X-100 in PBS for 10 min, washed again  
16 with PBS, and then incubated in skim milk blocking buffer (5% skim milk/2.5% goat  
17 serum/2.5% donkey serum/0.1% gelatin/PBS) or BSA blocking buffer (2% BSA in PBS) at  
18 room temperature for 1 h. Subsequently, the cells were incubated (room temperature, 1 h)  
19 with primary antibodies diluted with blocking solution, washed with PBS, and then probed

with secondary antibodies. Bacterial and cellular DNAs were stained with 4',6-diamidino-2-phenylindole (DAPI) (Dojindo, D523). All fluorescence micrographs shown here are confocal images acquired using an FV1000 laser-scanning microscope (Olympus). For quantitative analysis, cell images were captured at random using the confocal microscope, and then colocalization was determined by calculating the Pearson's coefficient after tracing individual cells by using ImageJ software (National Institutes of Health).

### ***Transferrin uptake***

Cells were incubated with 5 µg/mL Alexa-594-labelled human transferrin (Invitrogen Corporation, T13343) for 1 h at 37°C. Cells were washed with PBS and fixed, and the fluorescence intensity per cell was measured by confocal microscopy and ImageJ software. More than 10 randomly selected images were analyzed in each condition.

### ***Bacterial viability assay***

HeLa cells ( $4 \times 10^4$  cells/well) were cultured in 24-well culture plates and infected as described in "Bacterial infection." After an appropriate incubation period, cells were lysed in sterile distilled water and serial dilutions of the lysates were plated on THY agar plates. The number of invaded and surviving GAS was determined through colony counting. The invasion data are presented as the ratio of total intracellular GAS at 2 h to total adhered and internalized GAS at 1 h, and the survival data are presented as the ratio of intracellular live GAS at 4 h to total intracellular GAS at 2 h.



## ***Immunoprecipitation***

For immunoprecipitation, cells were harvested, washed with PBS, and lysed in a lysis buffer (10 mM Tris-HCl (pH 7.4), 150 mM NaCl, 10 mM MgCl<sub>2</sub>, 1 mM EDTA, and 1% Triton X-100) containing a proteinase inhibitor cocktail (Nacalai Tesque, 25955-11) for 30 min on ice. The lysates were centrifuged and the obtained supernatants were pre-cleared by incubating with Protein A Sepharose 4B (GE Healthcare Life Sciences, 17-1279-03) for 30 min at 4°C. After brief centrifugation, the supernatants were reacted with anti-FLAG or anti-GFP antibodies for 2 h at 4°C, and then Protein A Sepharose beads were added and allowed to react (with rotation) for 1 h at 4°C. The immunoprecipitates were collected by briefly centrifuging the mixtures, washed 5 times with lysis buffer, and analyzed through immunoblotting.

## ***Statistical analysis***

Colocalization and GcAV formation were quantified through direct visualization performed using confocal microscopy. Unless indicated otherwise, at least 50 GcAVs or 200 GAS-infected cells were counted per condition in each experiment, and at least 3 independent experiments were performed for each trial. Values, including those displayed in graphs, are means  $\pm$  SD. Statistical analysis was performed using a two-tailed Student's *t* test.  $P < 0.05$  was considered to indicate statistical significance; significance is marked as \* for  $P < 0.05$ , \*\* for  $P < 0.01$ , \*\*\* for  $P < 0.001$ , and NS for not significant.

1    **Acknowledgments**

2    This research was supported in part by Grants-in-Aid for Scientific Research (25293370,  
3    15K15130, 26462776, 16H05188), the funding program for Next Generation World-Leading  
4    Researchers (LS041) (I.N.), and the Daiichi Sankyo Foundation of Life Science (I.N.).

5

6    **Conflict of interest statement**

7    The authors declare that no competing interests exist.

8

9

10

## References

1. Mizushima N, Komatsu M. Autophagy: renovation of cells and tissues. *Cell* 2011; 147:728-41.
2. Tooze SA, Yoshimori T. The origin of the autophagosomal membrane. *Nat Cell Biol* 2010; 12:831-5.
3. Levine B. Eating oneself and uninvited guests: autophagy-related pathways in cellular defense. *Cell* 2005; 120:159-62.
4. Kuballa P, Nolte WM, Castoreno AB, Xavier RJ. Autophagy and the immune system. *Annu Rev Immunol* 2012; 30:611-46.
5. Deretic V, Levine B. Autophagy, immunity, and microbial adaptations. *Cell host & microbe* 2009; 5:527-49.
6. Nakagawa I, Amano A, Mizushima N, Yamamoto A, Yamaguchi H, Kamimoto T, et al. Autophagy defends cells against invading group A Streptococcus. *Science* 2004; 306:1037-40.
7. Yamaguchi H, Nakagawa I, Yamamoto A, Amano A, Noda T, Yoshimori T. An initial step of GAS-containing autophagosome-like vacuoles formation requires Rab7. *PLoS Pathog* 2009; 5:e1000670.
8. Nozawa T, Aikawa C, Goda A, Maruyama F, Hamada S, Nakagawa I. The small GTPases Rab9A and Rab23 function at distinct steps in autophagy during Group A

- 1 Streptococcus infection. *Cell Microbiol* 2012; 14:1149-65.
- 2 9. Haobam B, Nozawa T, Minowa-Nozawa A, Tanaka M, Oda S, Watanabe T, et al.
- 3 Rab17-mediated recycling endosomes contribute to autophagosome formation in response to
- 4 Group A Streptococcus invasion. *Cell Microbiol* 2014; 16:1806-21.
- 5 10. Hong W. SNAREs and traffic. *Biochim Biophys Acta* 2005; 1744:493-517.
- 6 11. Itakura E, Kishi-Itakura C, Mizushima N. The hairpin-type tail-anchored SNARE
- 7 syntaxin 17 targets to autophagosomes for fusion with endosomes/lysosomes. *Cell* 2012;
- 8 151:1256-69.
- 9 12. Furuta N, Fujita N, Noda T, Yoshimori T, Amano A. Combinational soluble
- 10 N-ethylmaleimide-sensitive factor attachment protein receptor proteins VAMP8 and Vti1b
- 11 mediate fusion of antimicrobial and canonical autophagosomes with lysosomes. *Mol Biol*
- 12 *Cell* 2010; 21:1001-10.
- 13 13. Darsow T, Rieder SE, Emr SD. A multispecificity syntaxin homologue, Vam3p,
- 14 essential for autophagic and biosynthetic protein transport to the vacuole. *J Cell Biol* 1997;
- 15 138:517-29.
- 16 14. Ishihara N, Hamasaki M, Yokota S, Suzuki K, Kamada Y, Kihara A, et al.
- 17 Autophagosome requires specific early Sec proteins for its formation and NSF/SNARE for
- 18 vacuolar fusion. *Mol Biol Cell* 2001; 12:3690-702.
- 19 15. Puri C, Renna M, Bento CF, Moreau K, Rubinsztein DC. Diverse autophagosome

- 1 membrane sources coalesce in recycling endosomes. *Cell* 2013; 154:1285-99.
- 2 16. Nair U, Jotwani A, Geng J, Gammoh N, Richerson D, Yen WL, et al. SNARE  
3 proteins are required for macroautophagy. *Cell* 2011; 146:290-302.
- 4 17. Mali P, Yang L, Esvelt KM, Aach J, Guell M, DiCarlo JE, et al. RNA-guided human  
5 genome engineering via Cas9. *Science* 2013; 339:823-6.
- 6 18. Wendler F, Tooze S. Syntaxin 6: the promiscuous behaviour of a SNARE protein.  
7 *Traffic* (Copenhagen, Denmark) 2001; 2:606-11.
- 8 19. Perera HK, Clarke M, Morris NJ, Hong W, Chamberlain LH, Gould GW. Syntaxin  
9 6 regulates Glut4 trafficking in 3T3-L1 adipocytes. *Mol Biol Cell* 2003; 14:2946-58.
- 10 20. Kuliawat R, Kalinina E, Bock J, Fricker L, McGraw TE, Kim SR, et al. Syntaxin-6  
11 SNARE involvement in secretory and endocytic pathways of cultured pancreatic beta-cells.  
12 *Mol Biol Cell* 2004; 15:1690-701.
- 13 21. Choudhury A, Marks DL, Proctor KM, Gould GW, Pagano RE. Regulation of  
14 caveolar endocytosis by syntaxin 6-dependent delivery of membrane components to the cell  
15 surface. *Nat Cell Biol* 2006; 8:317-28.
- 16 22. Laufman O, Hong W, Lev S. The COG complex interacts directly with Syntaxin 6  
17 and positively regulates endosome-to-TGN retrograde transport. *J Cell Biol* 2011;  
18 194:459-72.
- 19 23. Longatti A, Lamb CA, Razi M, Yoshimura S, Barr FA, Tooze SA. TBC1D14

- 1 regulates autophagosome formation via Rab11- and ULK1-positive recycling endosomes. J  
2 Cell Biol 2012; 197:659-75.
- 3 24. Watson RT, Pessin JE. Functional cooperation of two independent targeting  
4 domains in syntaxin 6 is required for its efficient localization in the trans-golgi network of  
5 3T3L1 adipocytes. J Biol Chem 2000; 275:1261-8.
- 6 25. Moore ER, Mead DJ, Dooley CA, Sager J, Hackstadt T. The trans-Golgi SNARE  
7 syntaxin 6 is recruited to the chlamydial inclusion membrane. Microbiology 2011; 157:830-8.
- 8 26. Kabeiseman EJ, Cichos KH, Moore ER. The eukaryotic signal sequence, YGRL,  
9 targets the chlamydial inclusion. Frontiers in cellular and infection microbiology 2014; 4:129.
- 10 27. Murray RZ, Wylie FG, Khromykh T, Hume DA, Stow JL. Syntaxin 6 and Vti1b  
11 form a novel SNARE complex, which is up-regulated in activated macrophages to facilitate  
12 exocytosis of tumor necrosis Factor-alpha. J Biol Chem 2005; 280:10478-83.
- 13 28. Manderson AP, Kay JG, Hammond LA, Brown DL, Stow JL. Subcompartments of  
14 the macrophage recycling endosome direct the differential secretion of IL-6 and TNFalpha. J  
15 Cell Biol 2007; 178:57-69.
- 16 29. Hulce JJ, Cognetta AB, Niphakis MJ, Tully SE, Cravatt BF. Proteome-wide  
17 mapping of cholesterol-interacting proteins in mammalian cells. Nature methods 2013;  
18 10:259-64.
- 19 30. Reverter M, Rentero C, Garcia-Melero A, Hoque M, Vila de Muga S,

- 1 Alvarez-Guaita A, et al. Cholesterol regulates Syntaxin 6 trafficking at trans-Golgi network  
2 endosomal boundaries. *Cell reports* 2014; 7:883-97.
- 3 31. Mounier J, Boncompain G, Senerovic L, Lagache T, Chretien F, Perez F, et al.  
4 *Shigella* effector IpaB-induced cholesterol relocation disrupts the Golgi complex and  
5 recycling network to inhibit host cell secretion. *Cell host & microbe* 2012; 12:381-9.
- 6 32. Taylor SD, Sanders ME, Tullos NA, Stray SJ, Norcross EW, McDaniel LS, et al.  
7 The cholesterol-dependent cytolysin pneumolysin from *Streptococcus pneumoniae* binds to  
8 lipid raft microdomains in human corneal epithelial cells. *PLoS One* 2013; 8:e61300.
- 9 33. Bhakdi S, Bayley H, Valeva A, Walev I, Walker B, Kehoe M, et al. Staphylococcal  
10 alpha-toxin, streptolysin-O, and *Escherichia coli* hemolysin: prototypes of pore-forming  
11 bacterial cytolysins. *Arch Microbiol* 1996; 165:73-9.
- 12 34. Kreykenbohm V, Wenzel D, Antonin W, Atlachkine V, von Mollard GF. The  
13 SNAREs vti1a and vti1b have distinct localization and SNARE complex partners. *Eur J Cell*  
14 *Biol* 2002; 81:273-80.
- 15 35. Guo B, Liang Q, Li L, Hu Z, Wu F, Zhang P, et al. O-GlcNAc-modification of  
16 SNAP-29 regulates autophagosome maturation. *Nat Cell Biol* 2014; 16:1215-26.
- 17 36. Mizushima N. Sugar modification inhibits autophagosome-lysosome fusion. *Nat*  
18 *Cell Biol* 2014; 16:1132-3.
- 19 37. Oda S, Nozawa T, Nozawa-Minowa A, Tanaka M, Aikawa C, Harada H, et al.

1 Golgi-Resident GTPase Rab30 Promotes the Biogenesis of Pathogen-Containing  
2 Autophagosomes. PLoS One 2016; 11:e0147061.

3

4



## Figure Legends

### **Figure 1.** STX6 localizes to TFRC-positive puncta on GcAVs.

(A) A screen for syntaxin (STX) proteins that colocalize with GcAVs. HeLa cells expressing EmGFP-fused STX proteins and mCherry-fused LC3 (GcAV marker) were infected with GAS for 4 h and fixed. The percentages of EmGFP-STX-positive GcAVs were measured using confocal microscopy. (B) GcAV localization of endogenous STX6. HeLa cells expressing EmGFP-LC3 (green) were infected with GAS for 4 h and stained for STX6 (red). DAPI labels the nuclei and GAS (blue). The insets show high-magnification views of the area outlined in the main merged image. (C) HeLa cells expressing mCherry-LC3 and EmGFP-STX6 were infected with GAS for 2 h. (D) Colocalization of STX6 with GcAVs at different times post-infection. HeLa cells expressing mCherry-LC3 and EmGFP-STX6 were infected with GAS for the indicated times, and the percentages of EmGFP-STX-positive GcAVs were measured using confocal microscopy. (E) Colocalization of STX6 with TFRC and GcAVs. HeLa cells expressing EmGFP-STX6 were infected with GAS for 4 h and then immunostained for TFRC. Scale bars, 10  $\mu$ m. (F) Pearson's coefficient quantified for STX6/TFRC colocalization on GcAVs. Data represent means  $\pm$  SD of >10 GcAVs analyzed per condition. (G) Merged image of the GcAV in (E). The graph shows the signal intensities of EmGFP-STX6 and TFRC measured along the red line in the GcAV image. Orange arrows indicate the signal peaks observed in both EmGFP-STX6 and TFRC. (H) Live-cell imaging

during GAS infection. HeLa cells expressing EmGFP-STX6 and mCherry-LC3 were infected with GAS for the indicated time points and images were captured by confocal microscopy. Scale bars, 3  $\mu$ m. Data in (A) and (D) are means  $\pm$  SD of 3 independent experiments.

**Figure 2.** STX6 regulates the fusion between REs and GcAVs.

(A) Immunoblotting analysis of STX6-knockdown HeLa cells. (B and C) HeLa cells transfected with control and STX6 miR vectors were infected with GAS for 4 h, fixed, and immunostained for TFRC. DAPI labels the nuclei and GAS. Representative confocal micrographs of GcAVs in control and STX6-knockdown (KD) HeLa cells (B), and quantification of TFRC-positive GcAVs (C). Yellow scale bars, 3  $\mu$ m. (D) Immunoblotting analysis of STX6-knockout (KO) HeLa cells. (E and F) HeLa wild-type (WT) cells, STX6-KO cells, and STX6-KO cells expressing FLAG-STX6 were transfected with EmGFP-LC3 and infected with GAS for 4 h. Cells were fixed and immunostained for TFRC. Representative confocal micrographs of GcAVs in WT and STX6-KO HeLa cells (E), and quantification of TFRC-positive GcAVs (F). (G and H) HeLa WT and STX6-KO cells expressing EmGFP-LC3 were infected with GAS for 4 h. Representative confocal micrographs of the HeLa cells of each type (G), and quantification of GcAV-positive cells (H). (I) HeLa WT and STX6-KO cells were infected with GAS for 1, 2, and 4 h. The number of invaded and surviving bacteria was measured in the GAS viability assay. Data in (C), (F), (H), and (I) are means  $\pm$  SD of 3 independent experiments.

**Figure 3.** VAMP3 and VTI1B interact with STX6 and promote the fusion between REs and GcAVs.

(A–C) HeLa cells expressing EmGFP-SNARE proteins and mCherry-LC3 were infected with GAS for 4 h, fixed, and immunostained for TFRC. Pearson's coefficient quantification of the colocalization of SNARE/LC3 or SNARE/TFRC on GcAVs (A), and representative confocal micrographs of VAMP3- and VTI1B-positive GcAVs (B, C). Data represent means  $\pm$  SD of >10 GcAVs analyzed per condition. Scale bars, 10  $\mu$ m. (D) STX6 interacts with VAMP3 and VTI1B. HeLa cells transfected with FLAG-STX6 and EmGFP (GFP), EmGFP-VAMP3, or EmGFP-VTI1B were either not infected or infected with GAS for 4 h, and then subjected to immunoprecipitations with an anti-GFP antibody. The immunoprecipitated proteins and total cell lysates were analyzed by immunoblotting with anti-FLAG and anti-GFP antibodies. (E) Immunoblotting analysis of VAMP3- and VTI1B-knockdown HeLa cells. (F and G) HeLa cells transfected with mCherry-LC3 and miR-control (Control), -VAMP3 (VAMP3 KD), or -VTI1B (VTI1B KD) were infected with GAS for 4 h and then fixed and immunostained for TFRC. Representative confocal micrographs of GcAVs in Control-, VAMP3 KD, and VTI1B KD HeLa cells (F), and Pearson's coefficient quantification of the colocalization of LC3/TFRC on GcAVs (G).

**Figure 4.** STX6 regions required for punctate localization on GcAVs, interaction with VAMP3 and VTI1B, and recruitment to GcAVs.

(A) Schematic map showing STX6 domain organization and deletion constructs used in this study. (B and C) HeLa cells transfected with EmGFP-STX6 constructs and mCherry-LC3 were infected with GAS for 4 h. Pearson's coefficient quantification of the colocalization of STX6 constructs/LC3 on GcAVs (B), and representative confocal micrographs of GcAVs (C). Scale bars, 10  $\mu$ m. (D) HeLa cells expressing EmGFP-STX6 $\Delta$ H2 and mCherry-LC3 were infected with GAS for 4 h and then immunostained for TFRC. The graph shows the signal intensities of EmGFP-STX6 and TFRC measured along the red line in the merged image. (E) STX6 H2 domain is required for interaction with VAMP3 and VTI1B. HeLa cells transfected with EmGFP-VAMP3 or -VTI1B and FLAG, FLAG-STX6, FLAG-STX6 $\Delta$ H1, or FLAG-STX6 $\Delta$ H2 were subjected to immunoprecipitations with an anti-FLAG antibody. The immunoprecipitated proteins and total cell lysates were analyzed by immunoblotting with anti-FLAG and anti-GFP antibodies. (F) HeLa STX6-KO cells expressing EmGFP-LC3 and FLAG-control, -STX6 FL, -STX6 $\Delta$ H2, or -STX6 $\Delta$ YGRL were infected with GAS for 4 h. The percentages of GcAV-positive cells were quantified using confocal microscopy. Data are the mean  $\pm$  SD of 3 independent experiments.

**Figure 5.** RABGEF1 is critical for the STX6-VAMP3 interaction and RE-GcAV fusion required to promote xenophagy.

(A) Immunoblotting analysis of STX6-KO HeLa cells. (B–D) Involvement of RABGEF1 in RE recruitment and GcAV formation. HeLa WT and RABGEF1-KO cells were transfected

with EmGFP-LC3 and FLAG-RABGEF1, infected with GAS for 4 h, and then fixed and immunostained for TFRC. Representative confocal micrographs of each cell type (**B**), and quantification of TFRC-positive GcAVs (**C**) and GcAV-positive cells (**D**). (**E** and **F**) Effects of RABGEF1 KO on GcAV localization of STX6, VAMP3, and VTI1B. HeLa WT and RABGEF1-KO cells were transfected with mCherry-LC3 and EmGFP-STX6, -VAMP3, or -VTI1B, and then infected with GAS for 4 h. Representative confocal micrographs of each cell type (**E**), and Pearson's coefficient quantification of colocalization on GcAVs (**F**). (**G** and **H**) RABGEF1 is required for the interaction between STX6 and VAMP3. HeLa WT and RABGEF1-KO cells were transfected with EmGFP-VAMP3 (**G**) or -VTI1B (**H**) and FLAG or FLAG-STX6, and subjected to immunoprecipitations with the anti-FLAG antibody. The immunoprecipitated proteins and total cell lysates were analyzed by immunoblotting with anti-FLAG and anti-GFP antibodies.

**Figure 6.** STX6 but not RABGEF1 is involved in starvation-induced autophagosome formation.

(**A** and **B**) WT and STX6 KO cells were cultured in regular or starvation medium for 2 h with or without E64d and pepstatin A, and analyzed by immunoblotting (**A**). The LC3-II level was quantified and normalized to that of actin (**B**). (**C** and **D**) WT and RABGEF1 KO cells were cultured in regular or starvation medium for 2 h with or without E64d and pepstatin A, and analyzed by immunoblotting (**C**). The LC3-II level was quantified and normalized to that of

1 actin (**D**). HeLa WT and STX6 KO cells stably expressing EGFP-LC3 were cultured in  
2 regular or starvation medium for 2 h. Confocal micrographs (**E**) and quantification of the  
3 number of LC3 puncta (**F**). Data in (**B**), (**D**), and (**F**) are the mean  $\pm$  SD of 3 independent  
4 experiments.

Figure 1

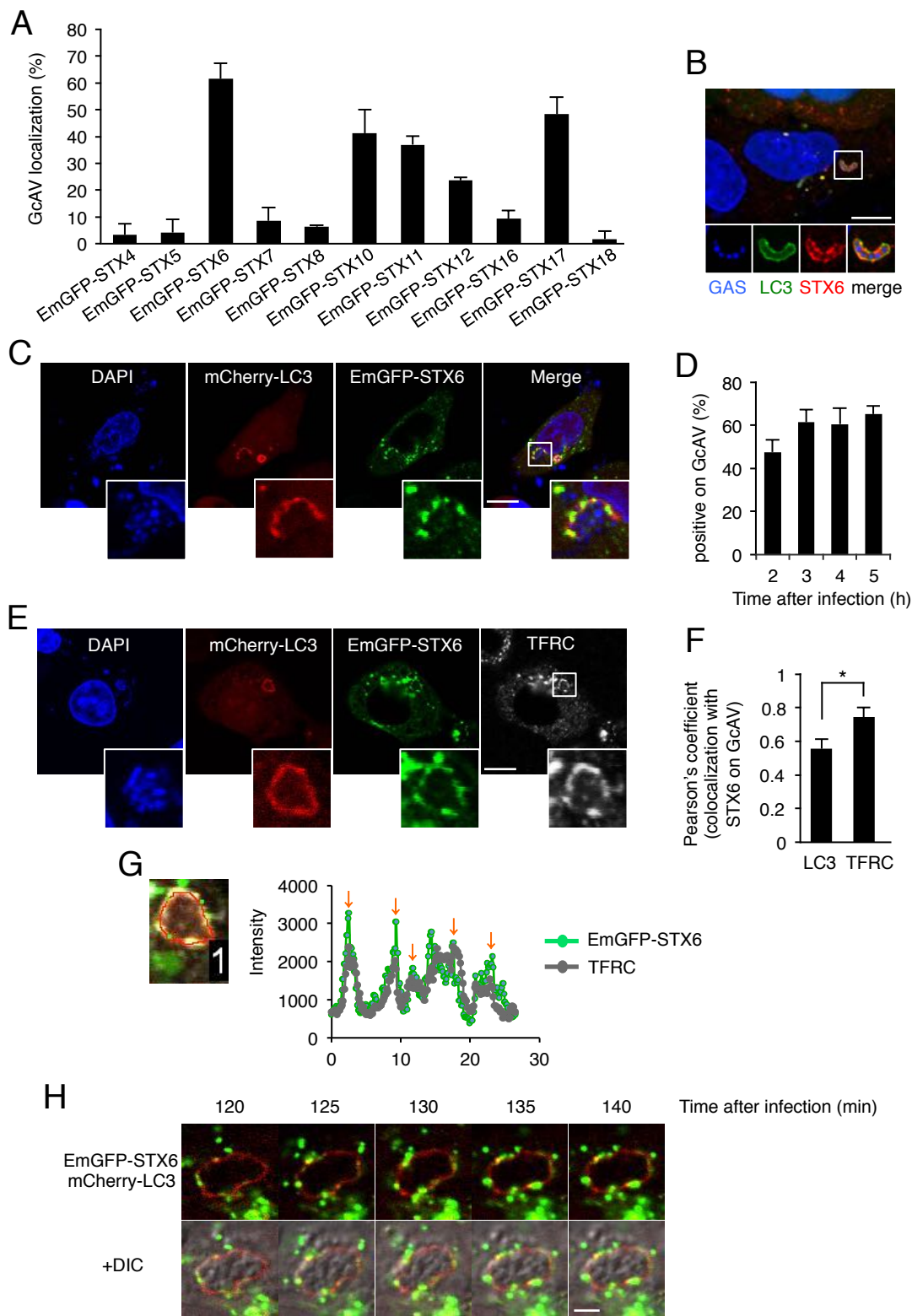


Figure 2

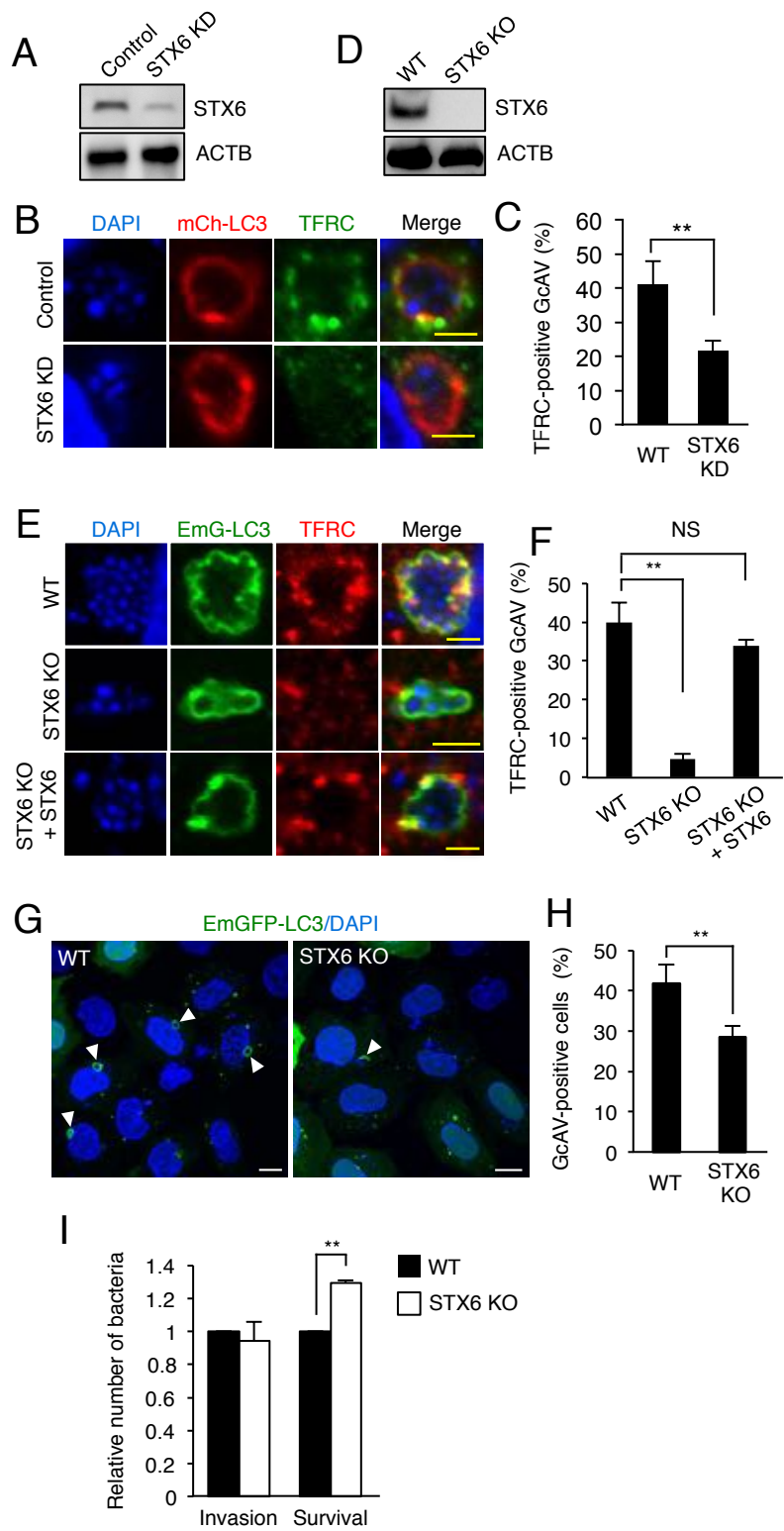




Figure 3

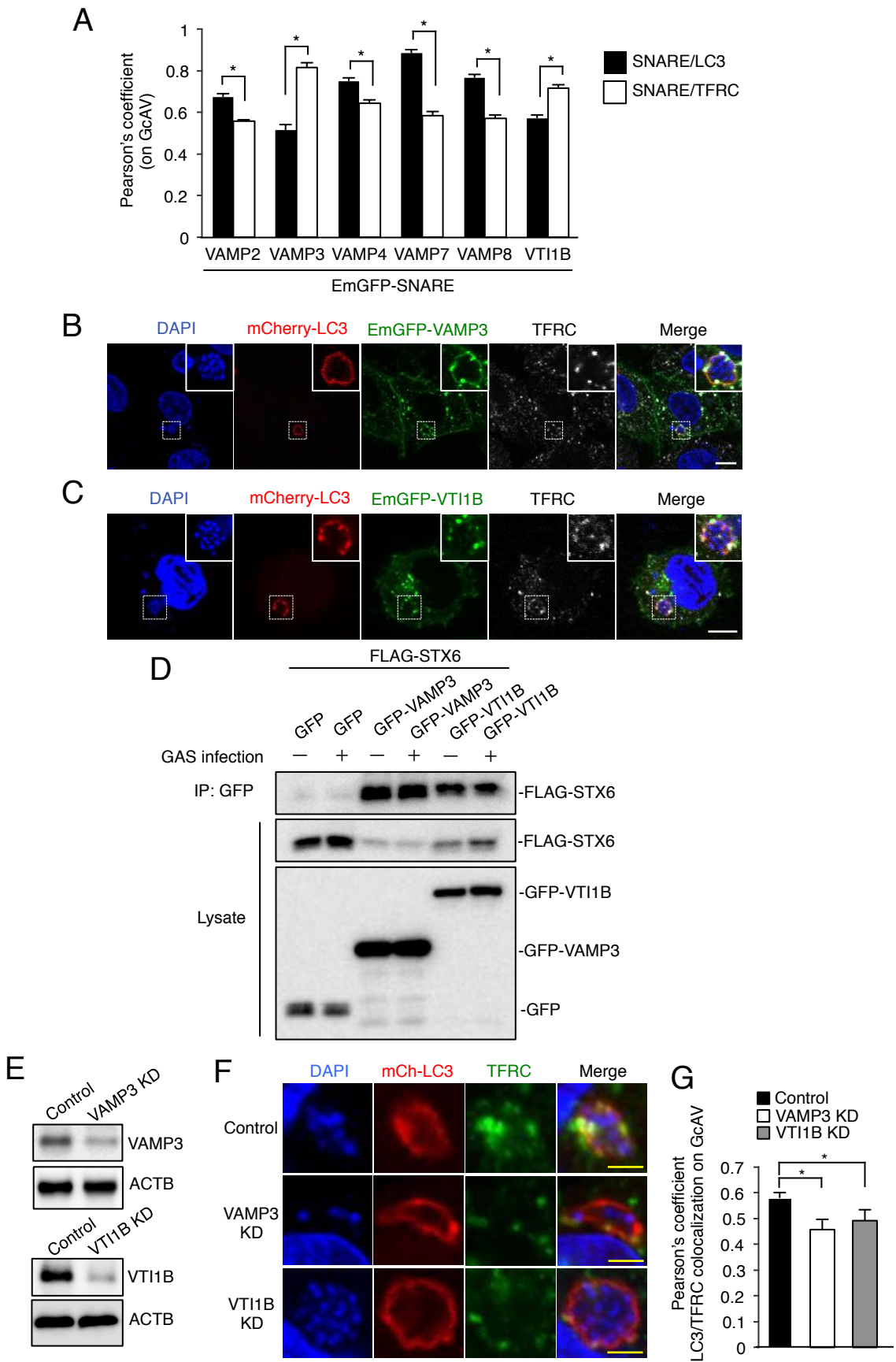


Figure 4

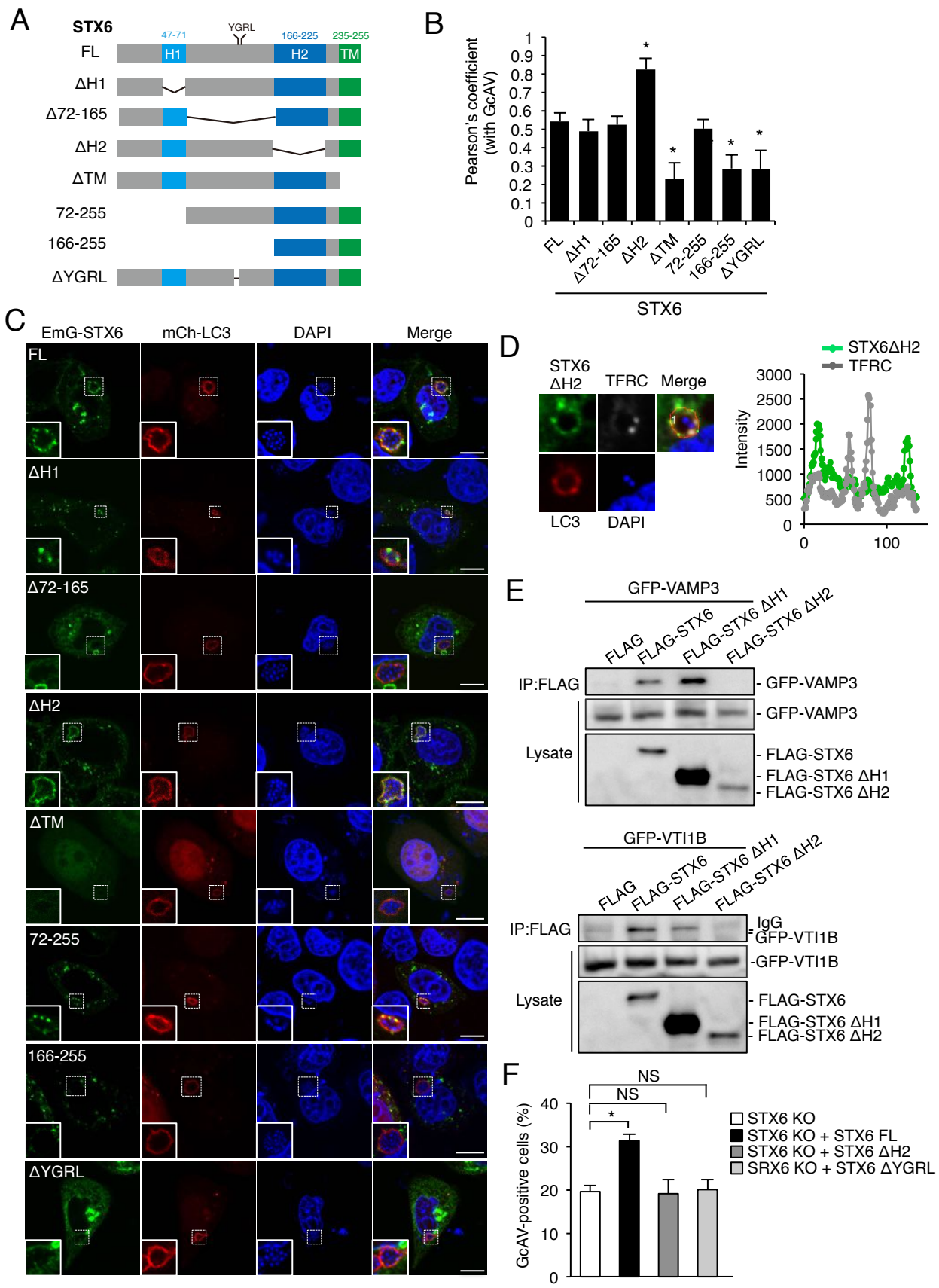


Figure 5

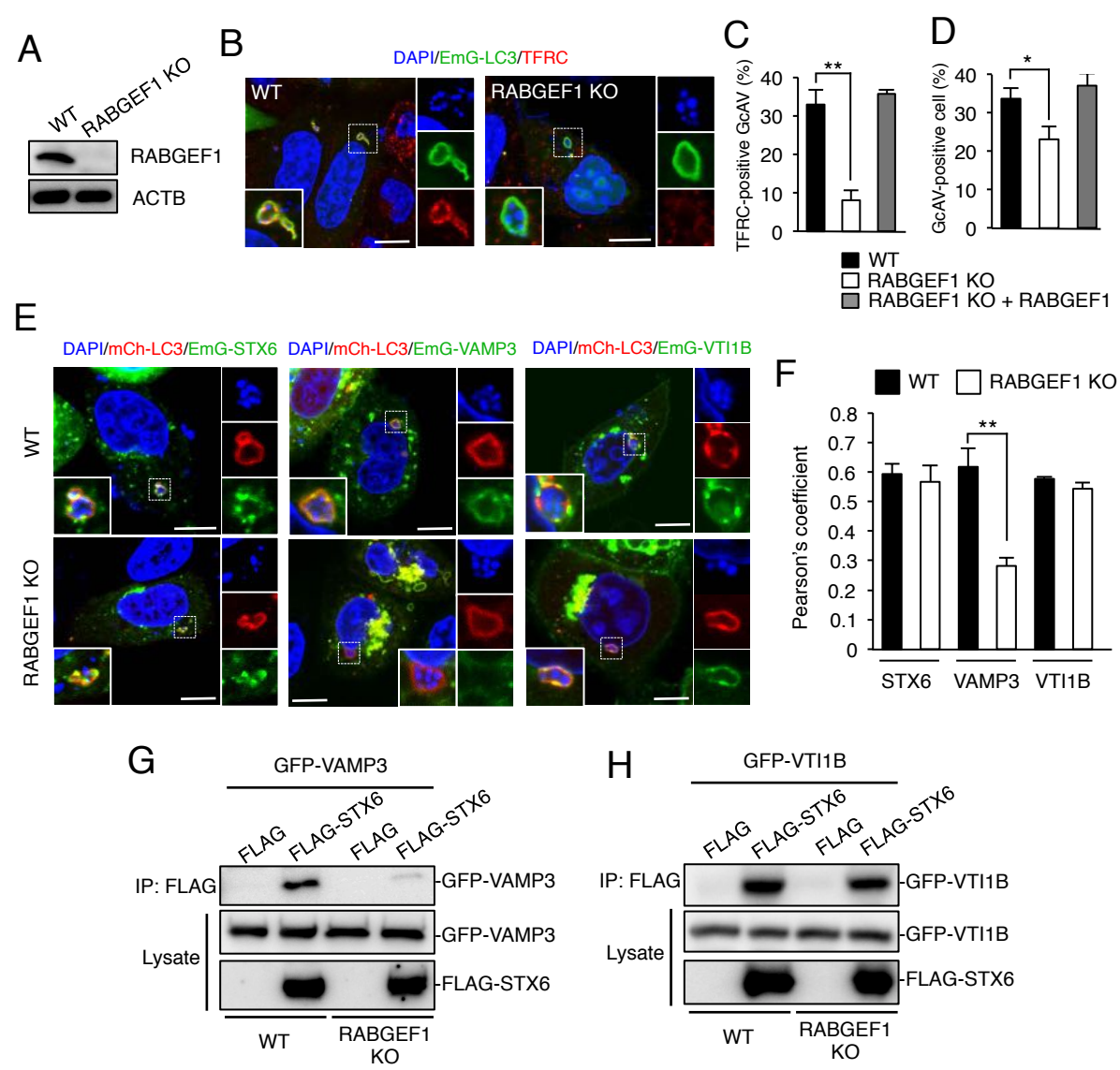
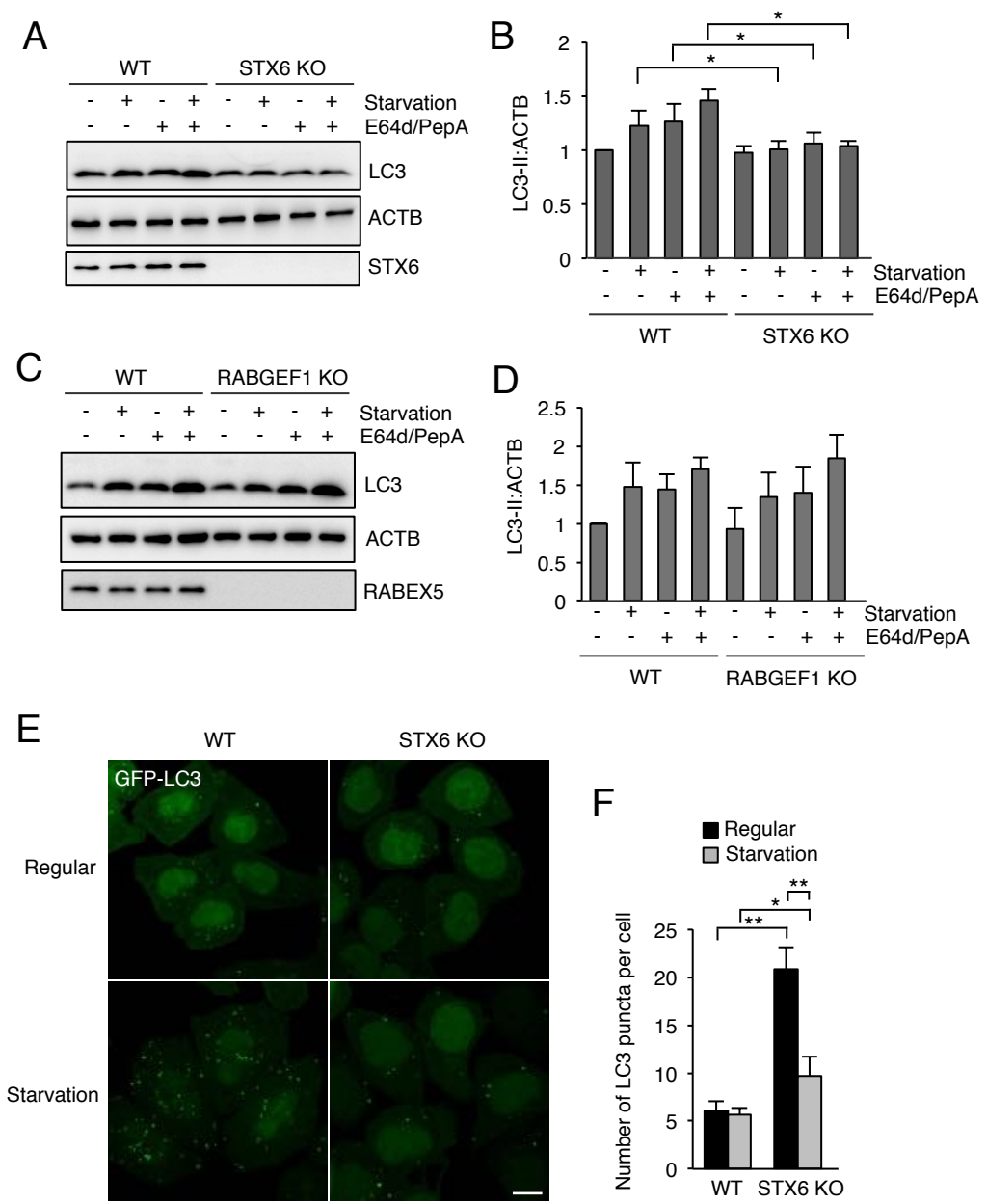
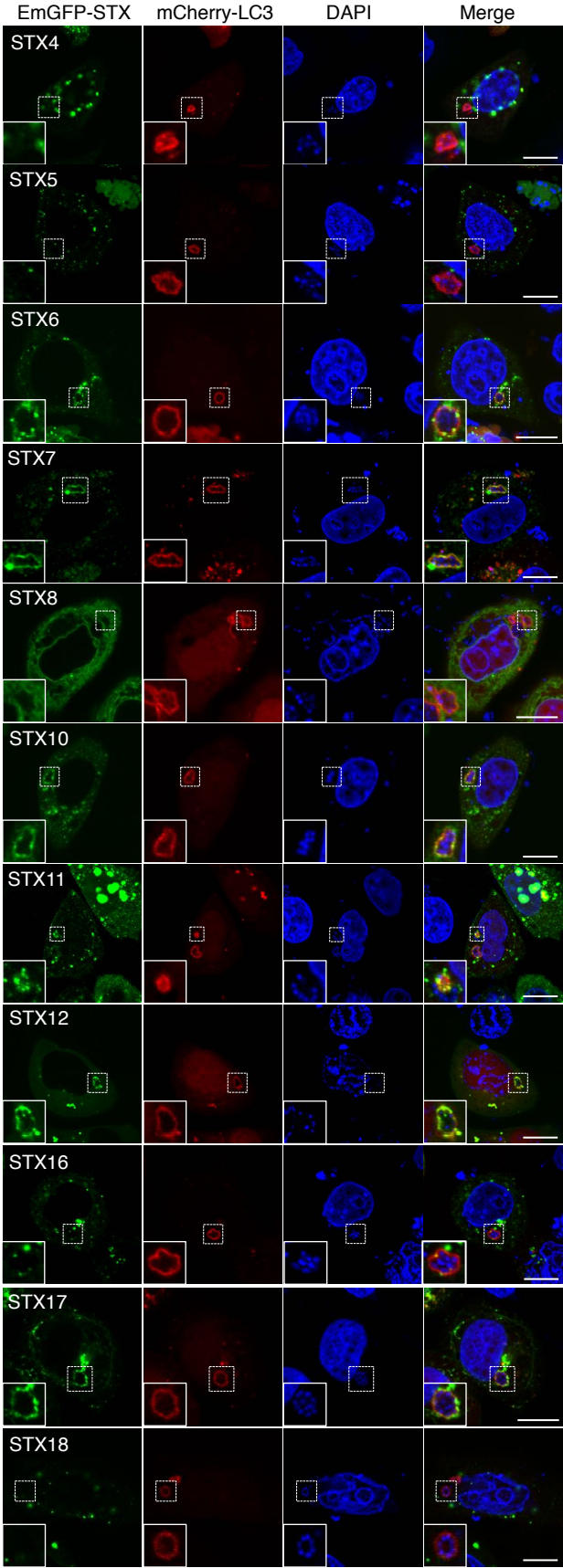


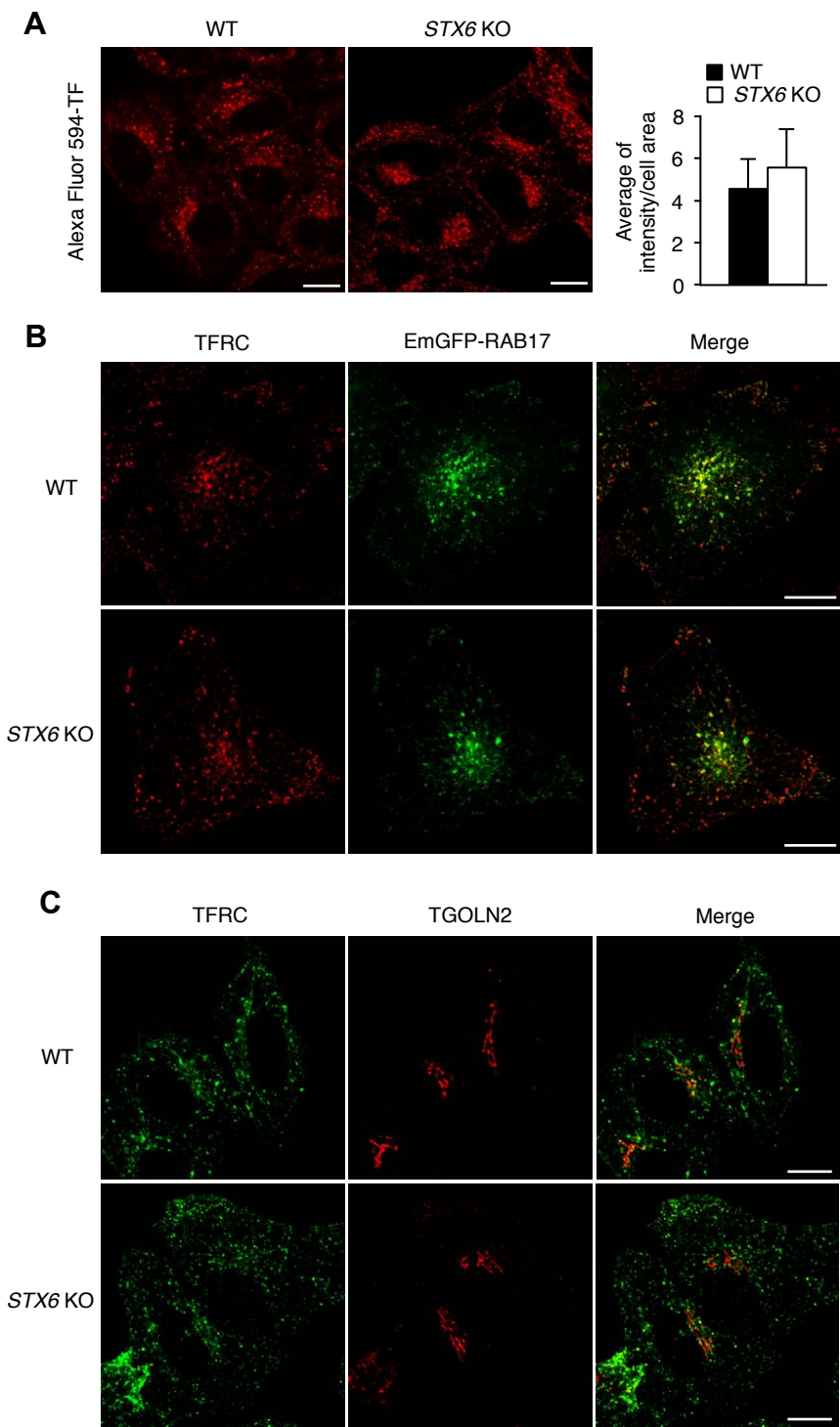
Figure 6



Supplementary Figure S1

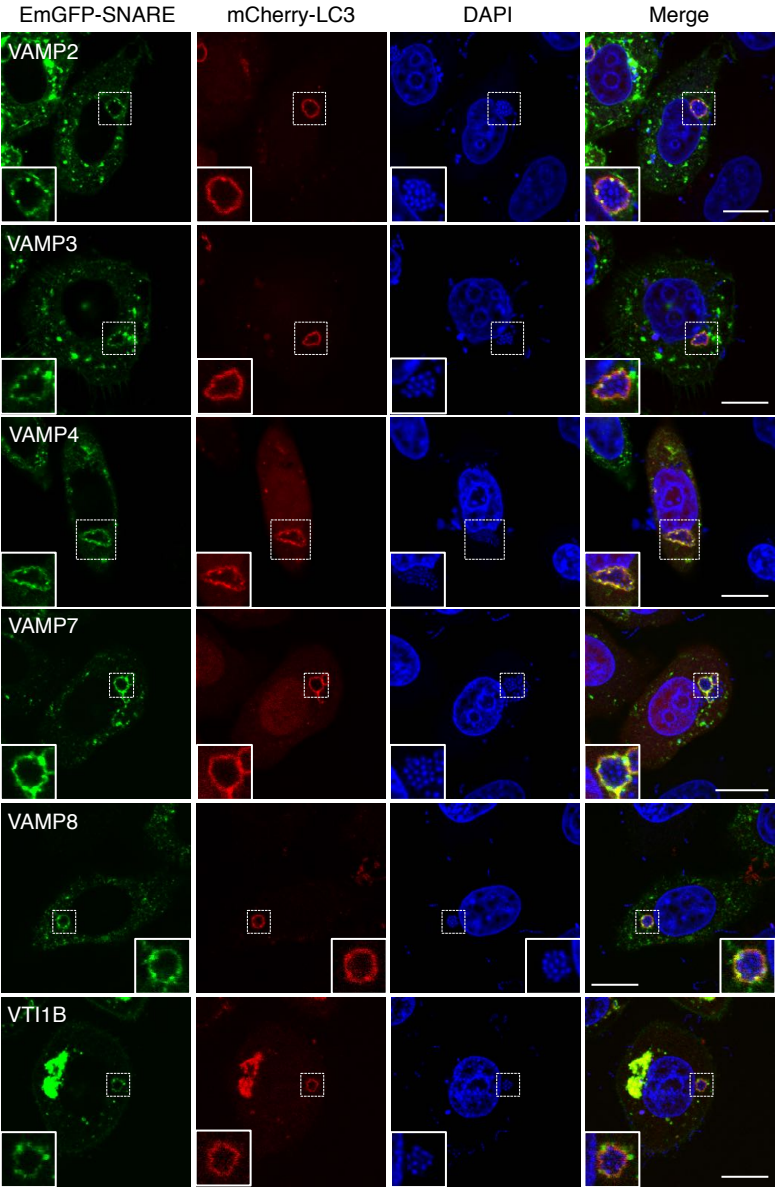


Supplementary Figure S2



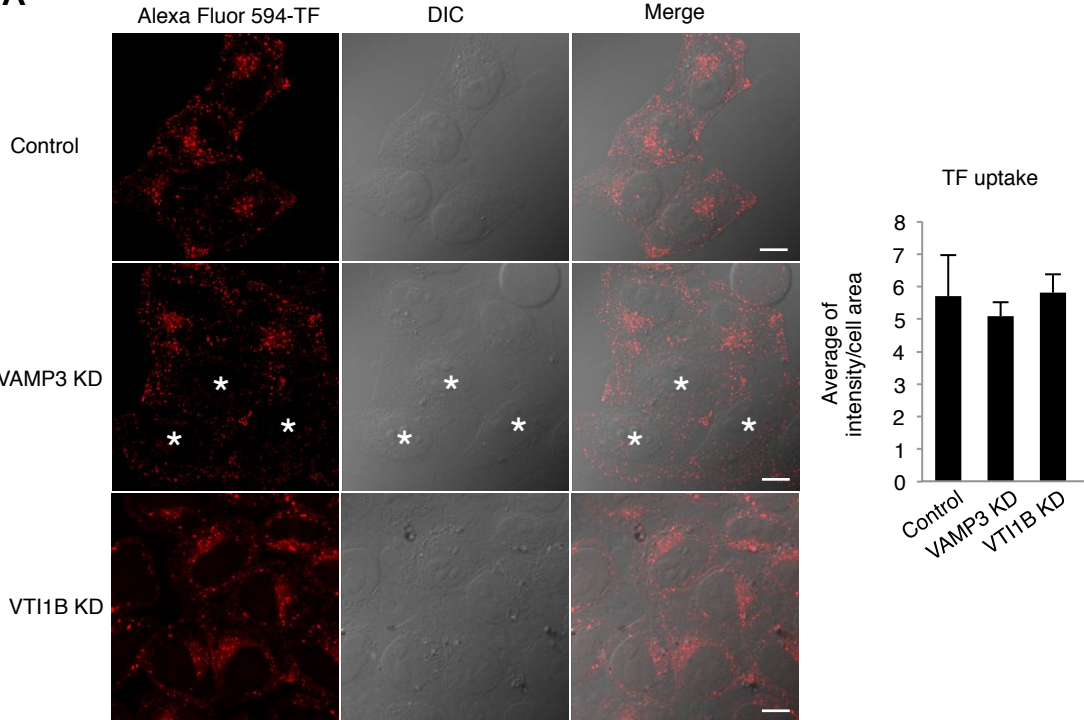


Supplementary Figure S3

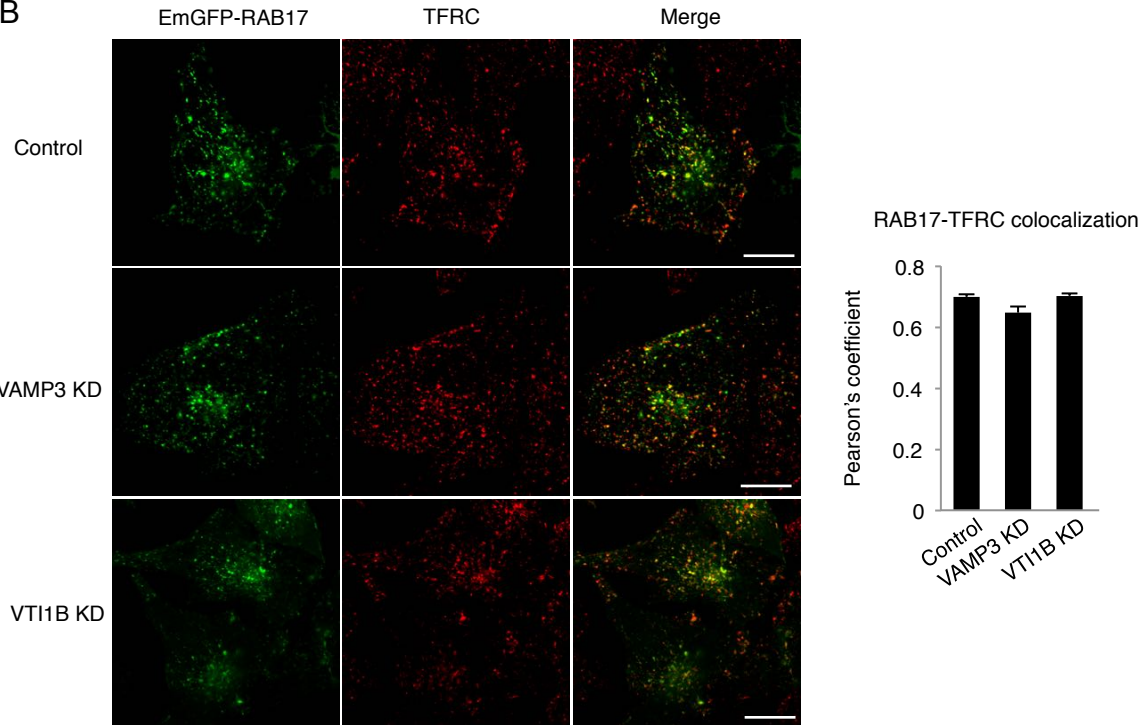


Supplementary Figure S4

**A**



**B**





Supplementary Figure S5

